Applied Catalysis B: Environmental 224 (2018) 80–87

Contents lists available at ScienceDirect

Applied Catalysis B: Environmental

journal homepage: www.elsevier.com/locate/apcatb

Research Paper

Nickel-doped sodium zirconate catalysts for carbon dioxide storage and hydrogen production through dry methane reforming process

J. Arturo Mendoza-Nieto[a,*], Samuel Tehuacanero-Cuapa[b], Jesús Arenas-Alatorre[b], Heriberto Pfeiffer[a,*]

[a] Laboratorio de Fisicoquímica y Reactividad de Superficies (LaFReS), Instituto de Investigaciones en Materiales, Universidad Nacional Autónoma de México, Circuito Exterior s/n, Ciudad Universitaria, Del. Coyoacán, CP 04510 Ciudad de México, Mexico

[b] Instituto de Física, Universidad Nacional Autónoma de México, Circuito Exterior s/n, Ciudad Universitaria, Del. Coyoacán, CP 04510, Ciudad de México, Mexico

ARTICLE INFO

Keywords:
CO_2 Chemisorption
Dry CH_4 reforming
NiO catalyst
Sodium zirconate
Syngas

ABSTRACT

NiO-doped sodium zirconate ceramics with different amounts of NiO (between 0 and 10 wt%) were synthetized and characterized by powder XRD, SEM-EDS and N_2 physisorption. Structural and microstructural characteristics of a Na_2ZrO_3 based-ceramic were maintained in all NiO-containing samples. These materials were tested for CO_2 capture (TGA), desorption processes (TPD) and dry CH_4 reforming (DMR, catalytic tests). Initially, samples were dynamically tested for CO_2 chemisorption; these tests showed a slight inhibition for CO_2 capture due to the presence of NiO, which partially blocked Na_2ZrO_3 surface sites where CO_2 can be chemisorbed. Then, NiO-doped samples were carbonated and exposed to a CH_4 flow in order to perform DMR reaction, using carbonate samples as CO_2 source. In all cases, NiO addition resulted in greater production of H_2 than that of pure Na_2ZrO_3. Additionally, a drastic reduction in the reaction temperature was observed, especially for NiO-doped Na_2ZrO_3 containing 10 wt% of NiO. Additionally, regeneration and cyclic behavior showed that it is possible to accomplish consecutive cycles of CO_2 capture-DMR with considerable Na_2ZrO_3 regeneration. On the other hand, cyclability was affected due to a partial NiO reduction after DMR steps. However, if a pre-oxidation step was performed, the catalytic activity and H_2 production were recovered. Hence, it was established that NiO-doped Na_2ZrO_3 materials can be used as bifunctional materials as (i) CO_2 captors and then as (ii) catalytic materials during DMR reaction.

1. Introduction

In recent decades, methane (CH_4) and carbon dioxide (CO_2) emissions have been responsible for climate change and global warming, as both gases are the major contributors to the greenhouse effect [1]. Although the concentration of methane in the atmosphere is much lower than that of CO_2, methane more effectively absorbs infrared radiation, and thus, its contribution to planet warming is significantly higher than that of CO_2 [2]. However, carbon dioxide emissions are the main contaminants and contribute almost 60% for enhancing greenhouse effect each year, whereas methane is the primary component of natural gas and is responsible for 15% of global warming [2–4]. One option for limiting greenhouse effects is to reduce the emission of both gases by converting them into an alternative and cleaner energy source. In this regard, hydrogen (H_2) production through the use of greenhouse gases would be a viable option [6–8]. Among H_2 production processes, the most commonly used are dry methane reforming (DMR) [9–12], steam methane reforming (SMR) [13,14], sorption-enhanced methane reforming (SEMR) [15–17], water-gas shift reaction (WGSR) [18–20] and ethanol-steam reforming (ESR) [21–23]. These processes all produce synthetic gas (syngas), which is composed of H_2 and carbon oxides (CO or CO_2), depending on the process utilized and reaction conditions. Hence, CO or CO_2 removal is usually a key step to purify H_2. Thus, different technologies have been developed over the past few years to accomplish this necessity [24].

In particular, dry CH_4 reforming does have some disadvantages: (1) the reforming reaction is highly endothermic; (2) high temperatures are required to obtain high conversions, which leads to catalyst deactivation by coke formation; and (3) the H_2 purity from this process is low, and additional operations, such as purification, separation and compression techniques, must to be used [25,26]. To achieve this goal, it has been necessary to use two different materials: one acting as a catalyst and a suitable chemical sorbent to eliminate the remaining CO_2 [16,17].

* Corresponding authors.
E-mail addresses: amendozan@comunidad.unam.mx, armeni86@hotmail.com (J.A. Mendoza-Nieto), pfeiffer@iim.unam.mx (H. Pfeiffer).

http://dx.doi.org/10.1016/j.apcatb.2017.10.050
Received 7 July 2017; Received in revised form 10 October 2017; Accepted 21 October 2017
Available online 03 November 2017
0926-3373/

In this sense, Ni-based catalysts supported over different metal oxides are the most used materials for performing DMR, *e.g.,* Ni/α-Al_2O_3 [9], Ni/γ-Al_2O_3 [10] or Ni/$Ce_xZr_{1-x}O_2$ [11]. On the other hand, CO_2 capture and storage (CCS) [5,27,28] can be achieved using different alkali (Li, Na and K) and earth-alkaline (Be, Mg and Ca) metal-based ceramics as chemical sorbents [29–34], as these CCS materials present high superficial basicity, good sorption-desorption kinetics, thermal stability, high regeneration ability, mechanical strength and selective CO_2 sorption [35].

Recently, sodium zirconate (Na_2ZrO_3) [36] and NiO-CaO composites [37] were synthetized, characterized and tested as possible bi-functional materials, acting as both CO_2 sorbents and then as catalysts for dry CH_4 reforming to obtain a consecutive CO_2 capture and DMR processes. Those results clearly showed that both materials capture CO_2, store it and then supply CO_2 during the DMR process (reaction (1)), thereby producing H_2 at T > 800 °C with Na_2ZrO_3; however, NiO-CaO showed a better catalytic behavior (~500 °C). With these results in mind, the aim of this work was to determine whether NiO addition modifies the CO_2 chemisorption on Na_2ZrO_3 as well as the catalytic activity for H_2 production through the DMR process.

$$CH_{4\ (g)} + CO_{2\ (g) desorbed from ceramic} \rightarrow 2\,H_{2\ (g)} + 2\,CO_{\ (g)} \quad (1)$$

2. Experimental section

2.1. Synthesis and characterization of NiO(x)-Na_2ZrO_3 materials

Sodium zirconate doped with different nickel oxide loadings were synthesized *via* acetate decomposition. Hereinafter, NiO-doped materials are labeled NiO(x)-Na_2ZrO_3, where x represents the NiO loading used (x = 0.0, 2.5, 5.0, 7.5 and 10 wt%). Sodium acetate ($NaC_2H_3O_2$, Aldrich), zirconium acetate solution in acetic acid ($Zr(C_2H_4O_2)_4$, 16.1 wt% Zr, Aldrich) and nickel acetate tetrahydrate ($Ni(C_2H_3O_2)_2{\cdot}4H_2O$, 98%, Aldrich) were used as reagents. Due to the likelihood of Na sublimation at temperatures higher than 800 °C, a 15.0 wt% excess of $NaC_2H_3O_2$ was considered [35,38]. Acetate precursors were dissolved in water and heated at 60 °C until a paste was obtained. A solid product was obtained after two stages of calcination in static air: (1) first, acetate decomposition was carried out *via* heating at 400 °C for 6 h, then (2) the sodium zirconate crystalline structure was obtained *via* heating at 900 °C for 12 h.

NiO-containing catalysts were structurally and microstructurally characterized by powder X-ray diffraction (XRD), N_2 adsorption-desorption and analytical scanning electron microscopy (SEM-EDS). XRD patterns were recorded in the 10° ≤ 2Θ ≤ 70° range with a goniometer speed of 1° (2Θ) min^{-1}, using a Siemens D5000 diffractometer coupled to a cobalt anode (λ = 1.789 Å) X-ray tube. Once the NiO(x)-Na_2ZrO_3 crystalline structures were determined, nitrogen adsorption-desorption isotherms were measured with a Bel-Japan Minisorp II equipment at 77 K using a multipoint technique. Prior to physisorption experiments, samples were degassed at room temperature for 12 h in vacuum ($p < 10^{-1}$ Pa). The specific surface area (S_{BET}) for each material was calculated with a BET model. CO_2 temperature-programmed desorption (TPD) analyses were performed using a chemisorption analyzer (Belcat, Bel-Japan). Before each analysis, approximately 50 mg of sample was introduced into a quartz cell and pretreated at 850 °C under a He flow (30 mL/min). Each sample was then cooled to 200 °C and saturated with a 60 mL/min flow of CO_2 for 60 min. Afterwards, CO_2-TPD analyses were performed by heating each sample up to 850 °C (heating rate of 2 °C/min) in a He flow, and the data were quantified by a thermal conductivity detector (TCD). Finally, scanning electron microscopy (SEM) coupled to energy dispersive X-ray spectroscopy (EDS) measurements were recorded on a FE-SEM JEOL JSM 7800F electron microscope equipped with an energy dispersive analysis detector Oxford 50 mm^2 X-Max. The acceleration voltage used was 20 kV and a backscattered electron detector.

2.2. CO_2 capture and DMR processes

Carbon dioxide capture tests were performed in a Q500HR thermobalance from TA Instruments. NiO(x)-Na_2ZrO_3 samples were heat-treated dynamically from room temperature to 950 °C (heating rate of 3 °C/min). These experiments were performed using ~40 mg of sample and a carbon dioxide (CO_2, Praxair grade 3.0) flow rate of 60 mL/min. After CO_2 capture analysis, NiO(x)-Na_2ZrO_3 catalysts were tested in the dry reforming reaction (DMR) following a previously published procedure [36], using 200 mg of sample in a Bel-Rea catalytic reactor from Bel-Japan. First, NiO-doped samples were carbonated dynamically from 30 to 600 °C (heating rate of 5 °C/min) and then isothermally treated at 600 °C for 0.5 h. Finally, samples were cooled to 200 °C, using a gas mixture composed of 60 vol% CO_2 and 40 vol% N_2 (Praxair grade 4.8). Once samples were carbonated and partially cooled down to 200 °C, the dry methane reforming (DMR) process was performed from 200 to 900 °C (heating rate of 2 °C/min) using 100 mL/min of a gas mixture composed of CH_4 (5 vol%, Praxair grade 5.0) and N_2 balanced. In addition, cyclic experiments of CO_2 capture and subsequent DMR tests were performed with the NiO(10)-Na_2ZrO_3 catalyst. This procedure was performed using the same experimental conditions described above during 5 cycles, adding a sixth cycle, where CO_2 capture and DMR processes were performed after a previous oxidation step under 30 mL of O_2 at 600 °C for 2 h. Reforming gas products were analyzed every 15 °C up to 900 °C (dynamic experiments), or every 8.3 min (isothermal experiments), using a Shimadzu GC-2014 gas chromatograph with a Carbonex-1000 column. After DMR isothermal experiments, some materials were re-characterized by XRD.

3. Results and discussion

3.1. Characterization of NiO(x)-Na_2ZrO_3 materials

Powder XRD patterns for NiO(x)-Na_2ZrO_3 samples (0 ≤ x ≤ 10) are shown in Fig. 1. As expected, Na_2ZrO_3 crystalline planes were observed (PDF file 35-0770) in the pure sample (x = 0.0). X-ray patterns for Na_2ZrO_3 materials doped with different NiO amounts showed the same sodium zirconate crystalline structure. However, Na_2ZrO_3 reflections shifted as a function of nickel oxide content, which indicate some changes in the crystalline unit cell. In addition to Na_2ZrO_3 crystalline variations, these XRD patterns presented three other reflections located at 43.8, 50.9 and 74.6°, in 2θ scale, which increased as a function of the

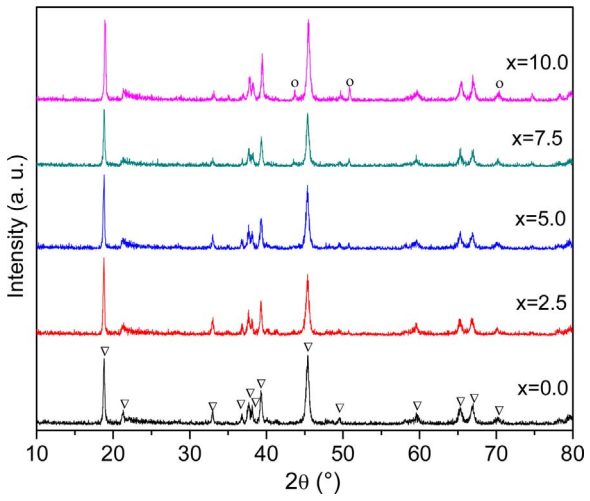

Fig. 1. NiO(x)-Na_2ZrO_3 XRD patterns. Crystalline phases were labeled as; (▽) Na_2ZrO_3 and (○) NiO.

Table 1
NiO(x)-Na_2ZrO_3 cell parameters determined from XRD data.

NiO loading	Cell parameters				Cell volume (Å^3)
	a (Å)	b (Å)	c (Å)	β (°)	
0.0	11.104 (2)	9.732 (1)	5.631 (4)	99.60 (2)	600.0 (4)
2.5	11.109 (2)	9.736 (1)	5.633 (4)	99.73 (2)	600.6 (4)
5.0	11.116 (2)	9.741 (1)	5.653 (4)	99.75 (2)	603.4 (4)
7.5	11.116 (2)	9.733 (1)	5.651 (4)	99.87 (2)	602.5 (4)
10.0	11.108 (2)	9.732 (1)	5.603 (4)	99.74 (2)	597.0 (4)

NiO loading used. These reflections are related to NiO formation (PDF file 65-5745). Furthermore, average crystallite size was estimated for NiO(10)/Na_2ZrO_3 sample by using Scherrer correlation and the (0 1 2) reflection located 50.9° in the 2θ scale, obtaining a NiO crystallite size equal to 52.1 nm. In an effort to further analyze the XRD patterns, cell parameters were calculated for NiO(x)-Na_2ZrO_3 samples (Table 1). It was observed that all unit cell parameters depend on nickel loading, presenting NiO-doped samples higher values than pure Na_2ZrO_3, excepting for c parameter which displays the largest variations in NiO (10)-Na_2ZrO_3 sample. The greatest cell expansion was observed with nickel loadings less or equal to 5 wt%. This result indicates that nickel incorporation into crystalline structure was possible at $x \leq 5.0$ wt%, which seems to be the solubility limit. In contrast, samples prepared with higher nickel loadings than 5.0 wt% presented a cell contraction, suggesting that part of nickel atoms were incorporated into Na_2ZrO_3 crystalline structure and the rest formed a secondary phase that according to previous XRD patterns corresponds to NiO formation over ceramic surface.

SEM analysis with backscattered electrons and EDS elemental mapping were performed for only two NiO-doped samples: NiO(5)-Na_2ZrO_3 and NiO(10)-Na_2ZrO_3 (Fig. 2). SEM images show two different compounds: a Na_2ZrO_3 phase detected by XRD and a Na_2CO_3 phase formed due to air exposition during analysis. Both NiO-containing samples presented large and dense particles, with particle sizes between 5 and 40 μm with a polyhedral shape (Fig. 2A and D). Additionally, it seems that morphology characteristics did not change as a function of nickel content. Regarding EDS elemental mapping analyses, Fig. 2C and F shows that nickel oxide observed previously by XRD (Fig. 1) is homogeneously distributed over the sodium zirconate surface, allowing a suitable dispersion of metallic particles in both cases.

In a further characterization, a N_2 physisorption technique was applied to determine the textural characteristics of the NiO(x)-Na_2ZrO_3 samples. Nitrogen adsorption-desorption isotherms are shown in Fig. 3. According to IUPAC classification, all materials present type II isotherms related to nonporous materials [39]. In these materials, no significant hysteresis loops were observed. Additionally, specific surface area (S_{BET}) was determined from N_2 adsorption curves using the BET model. The S_{BET} values were between 0.3 and 0.6 m^2/g, which are in line with synthesis method used. Additionally, N_2 physisorption results are in good agreement with previous reports for Na_2ZrO_3 materials [35,40,41]. Hence, nickel addition does not significantly modify Na_2ZrO_3 textural properties.

3.2. Carbon dioxide capture, storage and desorption

Once the NiO(x)-Na_2ZrO_3 samples were characterized; they were thermally treated from 30 to 950 °C under CO_2 flow into a thermobalance. Thermograms are shown in Fig. 4. All profiles exhibit a similar bimodal distribution as a function of temperature. First, an initial weight increase is observed between 100 and 400 °C, which is associated with CO_2 a chemisorption process over the Na_2ZrO_3 particle surfaces, according to previous reports [41,42]. In this step, a thin Na_2CO_3-ZrO_2 external shell is formed only over Na_2ZrO_3 particles (reaction (2)). It should be noted that all nickel-containing samples presented a lower superficial carbonation than that observed in the Na_2ZrO_3 case. This carbonation decrement must be totally related to nickel oxide formation which was not incorporated into the Na_2ZrO_3 structure (see XRD results) but instead on the Na_2ZrO_3 particle surface, reducing CO_2 sorption sites.

$$xNiO - Na_2Zr_{1-x}O_{3(s)} + CO_{2(g)} \rightarrow Na_2CO_{3(s)} + Zr_{1-x}O_{2(s)} + xNiO_{(s)} \quad (2)$$

All thermograms show a second weight increase at temperatures above 450 °C. This distribution is at least six or seven times greater than the superficial process discussed above and represents the highest amount of CO_2 captured (between 16.1–18.7 wt%). Weight increases in this temperature range are associated with activation of different diffusion processes [43], allowing bulk CO_2 chemisorption. This second CO_2 capture process was not affected by the nickel presence superficial, as NiO, or structurally into the Na_2ZrO_3 structure. In fact, curve slopes observed in this section did not vary significantly. Finally, in all NiO-containing materials, CO_2 desorption phenomena which registered in other Na_2ZrO_3 materials at approximately 800–850 °C [41,42], were not observed until 950 °C even in a pristine Na_2ZrO_3 sample. This result may be related to the low S_{BET} obtained in synthetized samples. In this case, a Na_2ZrO_3 ceramic synthetized without NiO addition demonstrated the best thermal behavior among all samples tested in the capture experiments and resulted in the highest amount of CO_2 chemisorbed (18.7 wt%) at 950 °C. Furthermore, Fig. 4 shows that an increase in the NiO composition causes a CO_2 chemisorption decrease of 1–3 wt% over the entire temperature range. Despite this decrease, NiO (x)-sodium zirconate materials chemisorbed between 16.1 and 17.7 wt % of CO_2 at 950 °C. Theoretical maximum capture values were calculated as a function of NiO content considering reaction (2), 23.8 wt% for x = 0.0 and 23.3 wt% for x = 10.0. Then, efficiencies were calculated as a ratio between experimental and theoretical values, obtaining values between 68–75% as NiO content (x) increases from 2.5 to 10.0%, while pure Na_2ZrO_3 (x = 0.0) presented an efficiency of 79%. As it can be seen, nickel addition produces a maximum efficiency reduction of 11%; this reduction may not be so important if nickel oxide contributes catalytically during DMR (see next Section 3.3).

CO_2-TPD experiments were performed with different NiO(x)-Na_2ZrO_3 samples in order to determinate the effect of NiO addition on CO_2 desorption abilities (Fig. 5). Regardless of the NiO content used, TPD profiles exhibit two desorption steps. The first one is located between 200 and 260 °C with a maximum approximately 225 °C, which is ascribed to a superficial chemisorption on Na_2ZrO_3 type materials (weakly bound CO_2). This desorption step shows almost the same thermal behavior in all samples. Meanwhile, the second signal shows the highest CO_2 desorption (550 and 850 °C), which can be attributed to a stronger bound CO_2 sorption over ceramic particles. For this step, it was observed that nickel addition induces a progressive reduction into CO_2 desorption temperature. Thus, NiO(10)-Na_2ZrO_3 sample showed CO_2 desorption which began at 550 °C with a maximum located at 765 °C, whereas pure Na_2ZrO_3 (x = 0.0) showed the highest temperature values (CO_2 desorption began at 650 °C with a maximum at 800 °C) among all samples tested. After TGA and TPD results, it was established that all NiO(x)-Na_2ZrO_3 materials, containing nickel oxide or not, are able not only to capture CO_2 but also able to store and desorb it over wide temperature range; therefore, NiO(x)-Na_2ZrO_3 materials are proposed as potential carbonated materials for other catalytic applications such as DMR process (reaction (1)).

3.3. Dry methane reforming (DMR)

After CO_2 capture and desorption analyses, a two-step process was performed to produce syngas (H_2 + CO). This process consisted of CO_2 capture at 600 °C on NiO(x)-Na_2ZrO_3 materials followed by a catalytic conversion between CH_4 and the previously captured CO_2. Notably, the carbonation process was performed at 600 °C, in line with previously

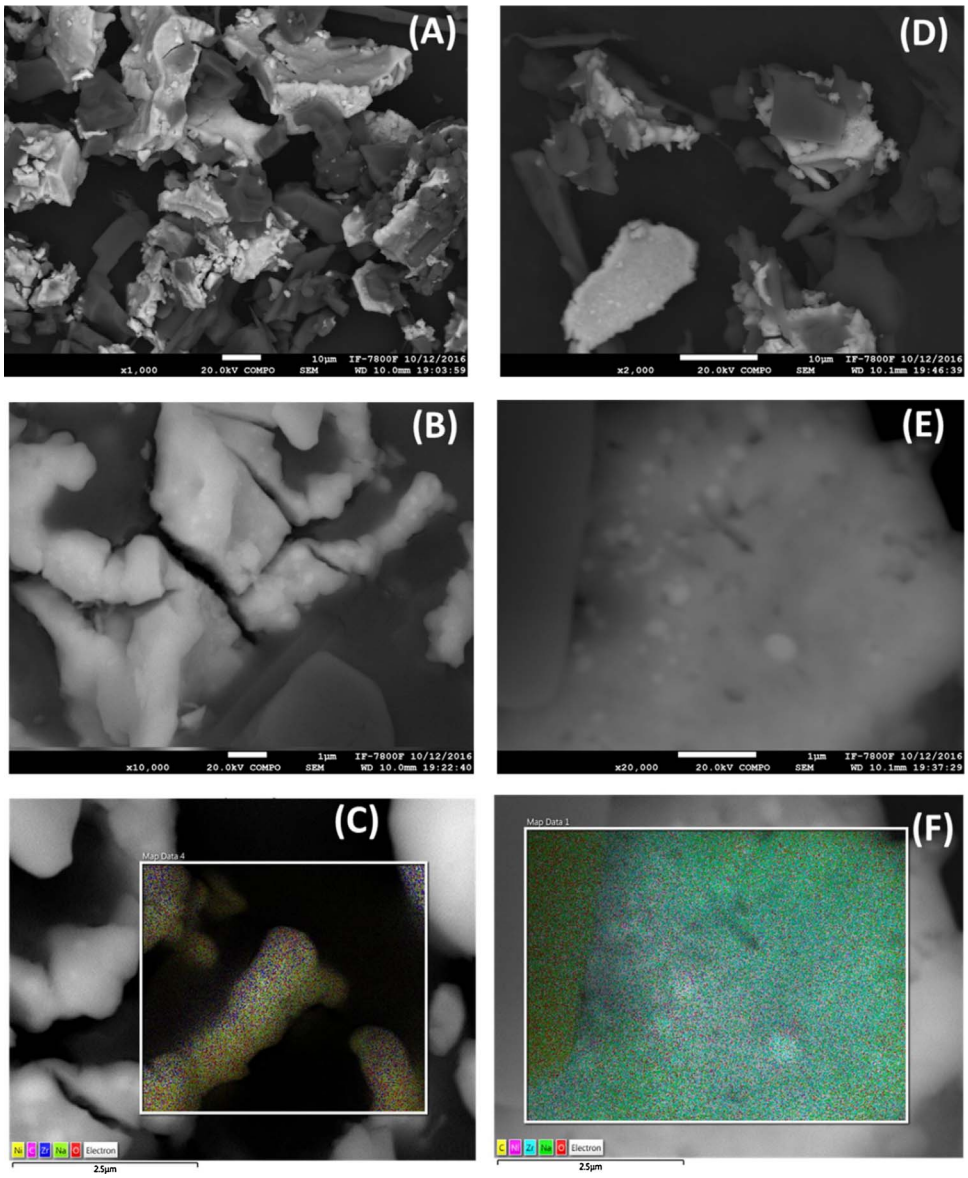

Fig. 2. SEM images and EDS elemental mapping for NiO(5)-Na_2ZrO_3 (A–B and C) and NiO(10)-Na_2ZrO_3 (D–E and F) materials.

published methods [36], where it was posed that at this temperature, Na_2ZrO_3 presents the highest CO_2 chemisorption. Fig. 6 shows reactants (CH_4 and CO_2) and products (H_2 and CO) evolution as a function of temperature for the Na_2ZrO_3 and NiO(10)-Na_2ZrO_3 samples. When the Na_2ZrO_3 sample was tested, H_2 production was detected from 785 °C, indicating that CH_4 reforming process occurs at relatively high temperatures. In fact, at higher temperatures, hydrogen formation became more evident, reached a 10% efficiency at 900 °C, and fit well with the CH_4 reduction content (Fig. 6A). It seems that hydrogen production is mainly generated at high temperatures through a partial CH_4 oxidation process, because CO_2 desorption from Na_2ZrO_3 sample occurred at a lower temperature range (600–850 °C), which indicated that desorbed CO_2 did not react with methane-producing syngas. This catalytic behavior is in good agreement with previous results [36], where similar H_2 amounts were obtained between 800 and 900 °C with a Na_2ZrO_3 material prepared *via* solid state method. Additionally, it can be observed that the H_2/CO ratio is lower than 1.0 from 700 to 860 °C, indicating that CO formation was greater than H_2 production, until the temperature reached $T > 870$ °C, where H_2/CO ratio was higher than 1.0. According to the literature [25], $H_2/CO < 1.0$ can be rationalized by the fact that the reverse water-gas shift reaction (where H_2 formed reacts with CO_2), occurred simultaneously with the DMR reaction.

In contrast, catalytic evolution for the carbonated NiO(10)-Na_2ZrO_3 sample showed a totally different behavior for the DMR reaction (Fig. 6B). H_2 production shows four maxima at 550, 650, 835 and 900 °C, reaching 11.3, 26.1, 18.6 and 20.9% efficiencies, respectively. At 550 and 650 °C, H_2 production is in good agreement to CO_2 desorption, and confirms the DMR reaction. Here, the CH_4 concentration decreased at those temperatures, while H_2 and CO increased. At higher temperatures ($T > 835$ °C), hydrogen and carbon monoxide production are observed, with a corresponding CH_4 reduction. However, CO_2 desorption was not detected, showing that at high temperatures, H_2 formation was produced due to partial CH_4 oxidation, as CO_2 seems to be absent in gas mixture. In contrast to the H_2/CO ratios obtained for the pure Na_2ZrO_3 sample, in all temperature ranges evaluated with the NiO(10)/Na_2ZrO_3 catalyst, it was observed that H_2/CO ratios were between 1.01 and 1.92, indicating that H_2 production is always higher than CO formation. Additionally, at some temperatures (600–635 and 665–720 °C), the H_2/CO ratio was almost equal to 1.0, suggesting that reverse water gas shift reaction was not possible [25]. The above results clearly show that using Na_2ZrO_3 with NiO drastically enhances syngas production in comparison to the use of pure Na_2ZrO_3 (Fig. 6A).

To understand the NiO effect on hydrogen production, a series of NiO(x)-Na_2ZrO_3 materials doped with different NiO loads

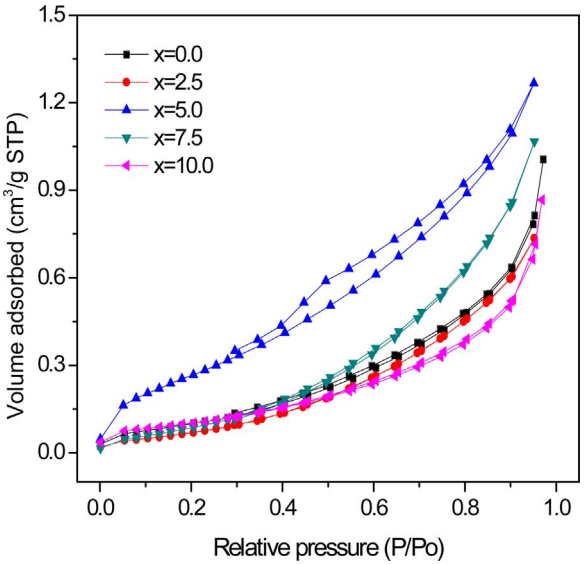

Fig. 3. N_2 adsorption-desorption isotherms at 77 K for NiO(x)-Na_2ZrO_3 materials prepared with different NiO loadings.

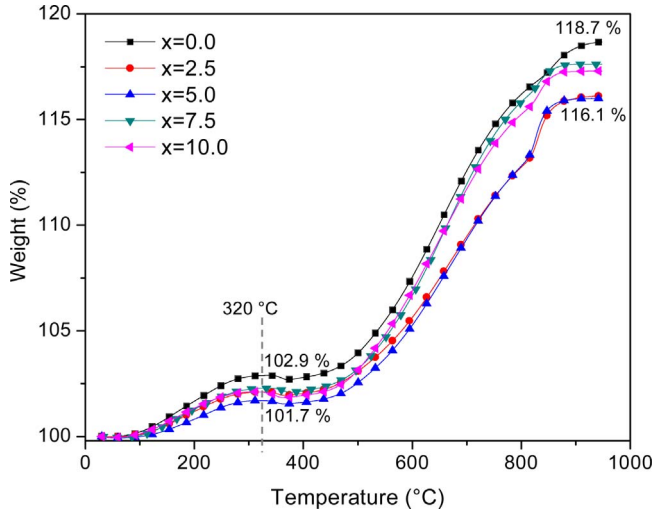

Fig. 4. Thermogravimetric analyses for NiO(x)-Na_2ZrO_3 samples tested dynamically from 30 to 900 °C in a saturated CO_2 atmosphere (60 mL/min).

(2.5 ≤ x ≤ 10) were tested in DMR reactions. Fig. 7 shows the thermal evolution for H_2 production using these NiO(x)-Na_2ZrO_3 catalysts. As can be seen, hydrogen formation and production temperature are a function of nickel content. In general, Ni addition not only causes an increase in H_2 formed, but also does so at lower temperatures. NiO(x)-Na_2ZrO_3 profiles exhibit some differences in comparison to pure Na_2ZrO_3 ceramic, as was described above. When sodium zirconate was doped with 2.5, 5.0 and 7.5 wt% of NiO, a bimodal profile was observed and is shown in Fig. 7. In addition to the temperature range for CH_4 reduction observed in pure Na_2ZrO_3 between 850 and 900 °C; another signal for H_2 production was detected in a lower temperature range (750–850 °C), increasing from 9.2% in the NiO(2.5)-Na_2ZrO_3 sample to 15.0% in the NiO(7.5)-Na_2ZrO_3 material. Not only was a larger amount of H_2 obtained as the Ni content increased but also the temperature decreased from 850 to 816 °C, consistent with the behavior observed during TPD analyses (see Fig. 5). Finally, when the highest amount of NiO (x = 10.0 wt%) was added to Na_2ZrO_3, the best catalytic behavior was observed in terms of a significant increase in hydrogen formation and a decrease in temperature. Therefore, the catalytic behavior observed at T < 800 °C can be due to DMR occurred over the NiO species

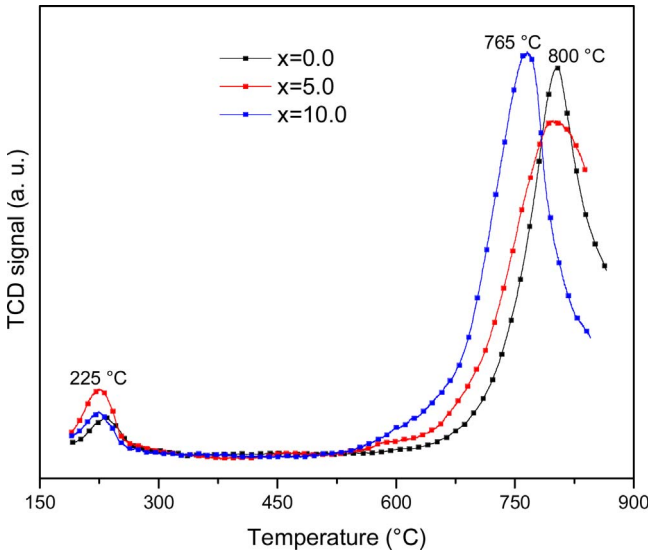

Fig. 5. CO_2-TPD desorption profiles for carbonated NiO(x)-Na_2ZrO_3 samples heat treated from 200 to 850 °C in a He flow.

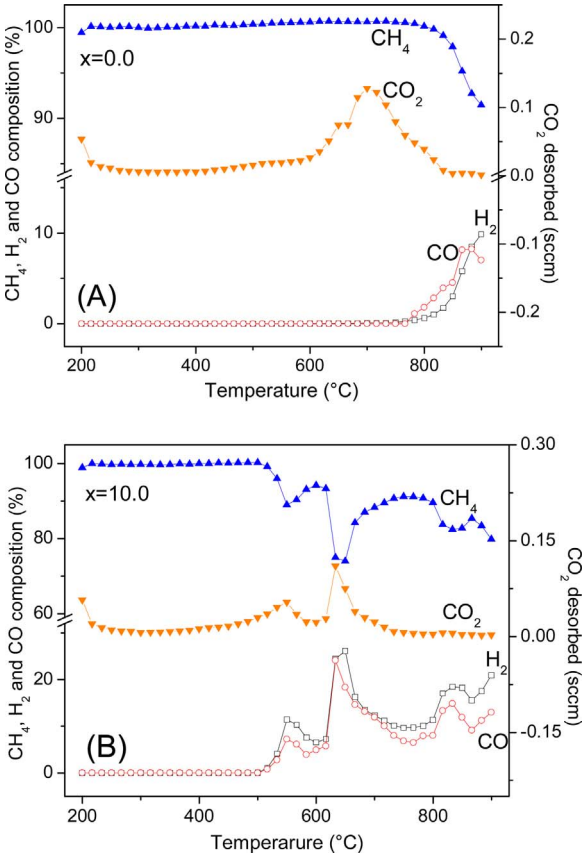

Fig. 6. Dynamic evolution (200–900 °C) for reactants (CO_2 and CH_4) and products (CO and H_2) obtained after CO_2 capture and CH_4 reforming processes using NiO(x)-Na_2ZrO_3 samples with different NiO compositions: (A) x = 0.0 and (B) x = 10.0. CO_2 average quantification is not possible as it was desorbed from the ceramics, thus it is only reported in sccm units.

located at of surface of sodium zirconate catalysts. A similar result had been previously observed for a DMR reaction using NiO-CaO composites. In that case, H_2 production occurred between 500 and 700 °C and it was ascribed to the NiO presence at the ceramic surface [37].

To analyze possible cyclability for NiO(10)-Na_2ZrO_3 sample during CO_2 capture and subsequent DMR, six cycles were performed with the

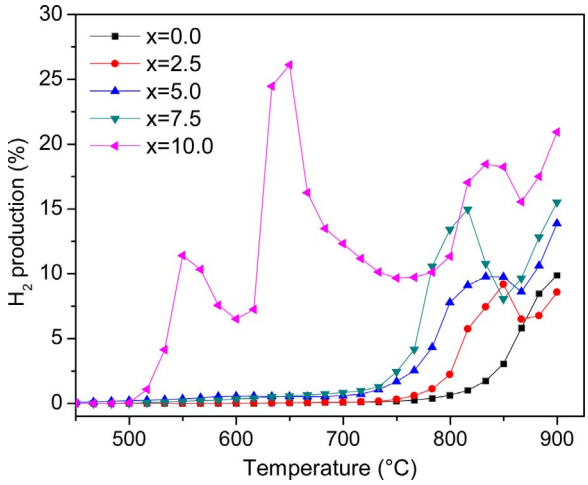

Fig. 7. Hydrogen formation obtained during dry methane reforming process, using NiO (x)-Na_2ZrO_3 catalysts with different Ni loadings.

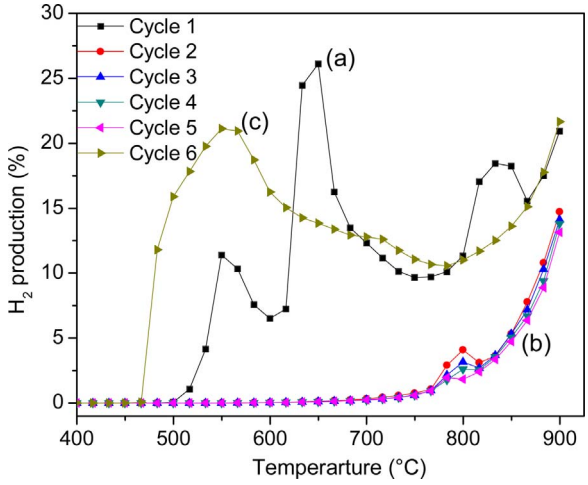

Fig. 8. Cyclic CO_2 carbonation-DMR tests, using a pristine NiO(10)-Na_2ZrO_3 material in cycle 1 (a), a reduced Ni(10)-Na_2ZrO_3 sample in cycles 2–5 (b) and a re-oxidized NiO(10)-Na_2ZrO_3 material in cycle 6 (c).

same physicochemical conditions previously described in the experimental section. Fig. 8 shows hydrogen formation as a function of temperature in each cycle. The catalytic performance between 800 and 900 °C did not change during cyclic tests. In contrast, catalytic behavior at T < 800 °C depends strongly on the number of cycles performed. H_2 production decreases drastically between the cycles 2 and 5, with H_2 formation lower than 5% in these cycles at approximately 800 °C. The main reason for this decrement may be due to NiO reduction to metallic nickel during DMR steps. To test whether the nickel oxidation state was responsible for this phenomenon, a sixth cycle was performed with a previous oxidation stage (see experimental section). The result showed that hydrogen production increases drastically between the fifth and sixth cycles, reaches the highest H_2 production (21.1%) at 550 °C and maintains the same catalytic behavior at T > 850 °C (Fig. 8). In fact, the temperature range for H_2 production improved as well. It means that DMR and partial oxidation processes were enhanced after catalyst oxidation stage, proving that the catalytic process highly depends on the oxidation state of nickel.

Finally, after CO_2 capture and the subsequent CH_4 reforming process, it should be determined whether sodium zirconate doped with 10 wt% of NiO could be regenerated through these processes as well as through the NiO reduction process. Thus, different sample products were analyzed by X-ray diffraction (XRD), where the pristine NiO(10)-Na_2ZrO_3 was included for comparison purposes (Fig. 9). When the NiO (10)-Na_2ZrO_3 sample was carbonated at 600 °C, the XRD pattern changed drastically and showed Na_2CO_3 (JCPDS card 37-0451) and ZrO_2 (JCPDS card 37-0451) formations, as could be expected. Differences in peak intensities between ZrO_2 and Na_2CO_3 phases are due to a gap in corresponding Zr and Na diffraction scattering coefficients. Finally, X-ray diffraction patterns for products obtained after one or six CO_2 capture-DMR cycles showed Na_2ZrO_3 as the main crystalline phase, as well as two ZrO_2 phases (tetragonal and monoclinic), as minor secondary phases. The above result clearly shows that a partial ceramic regeneration is produced after the CH_4 reforming reaction. However, the Na_2ZrO_3 regeneration degree depends on the number of cycles performed. On the other hand, two ZrO_2 crystalline phases were detected, indicating that part of the Na content was lost during cycle experiments, perhaps through Na sublimation during thermal Na_2CO_3 decomposition [44]. In the ZrO_2 tetragonal case, it may be produced by a Na-doped ZrO_2 structure [45]. Sodium sublimation may be controlled by reducing the final temperature reached in catalytic tests. Finally, it should be mentioned that metallic nickel could not be detected by XRD. Perhaps the amount or dispersion of metallic nickel did not allow its detection due to XRD detection limits.

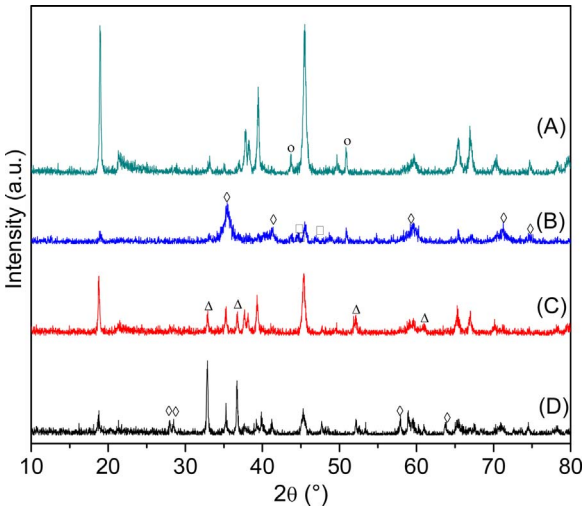

Fig. 9. XRD patterns for (A) original NiO(10)-Na_2ZrO_3, (B) dynamically carbonated-NiO (10)-Na_2ZrO_3 sample, (C) NiO(10)-Na_2ZrO_3 obtained after one cycle and (D) after six cycles of CO_2 capture-DMR. The secondary crystalline phases were labeled as: (○) NiO, (□) Na_2CO_3, (◊) tetragonal and (Δ) monoclinic ZrO_2.

4. Conclusions

In the present work, sodium zirconate materials doped with different nickel loads were synthetized, characterized and tested in two consecutive processes: (1) carbon dioxide capture and (2) DMR. According to characterization results (XRD, SEM-EDS and N_2 physisorption), it was possible to obtain NiO-doped Na_2ZrO_3 ceramics and maintain the main structure and characteristics of the sodium-containing ceramic. However, when the added NiO amount was greater than or equal to 7.5 wt%, it was not totally incorporated into the Na_2ZrO_3 crystal phase, forming NiO on the ceramic surface. After structural and microstructural characterization, the TG analysis showed that all Ni-containing materials can be used as CO_2 captors over a wide temperature range (200–900 °C), although the NiO presence slightly decreased the CO_2 chemisorption ability by 2–3 wt%, in comparison with Na_2ZrO_3. On the other hand, CO_2-TPD results showed that NiO addition promotes a significant decrease in Na_2ZrO_3 abilities for CO_2 desorption. In particular, a decrement of almost 100 °C was observed for the Na_2ZrO_3 sample prepared with 10 wt% of NiO.

All NiO(x)-Na_2ZrO_3 materials synthetized were carbonated and

subsequently used as a CO_2 source during DMR in order to produce syngas (CO + H_2). Catalytic results showed that all Ni-containing materials produced hydrogen and regenerate after the catalytic process. It was observed that increasing NiO resulted in a lowering of the catalytic temperature as well as a dramatic increase in the H_2 formed. Thus, the best catalytic behavior was obtained with Na_2ZrO_3 ceramic doped with 10 wt% of NiO. This sample produced H_2 over a wide temperature range (500–900 °C), optimal conditions occurred at 650 °C, where the highest H_2 formation was obtained, 26.1%. In fact, two different reactions generated syngas production: (i) DMR at T < 800 °C and (ii) partial CH_4 oxidation at T > 800 °C. Moreover, it was noticed that NiO (10)-doped material cyclability was reduced by means of NiO reduction to metallic Ni. Finally, it was found that performing an oxidation step after the DMR process promotes a re-oxidation of Ni, which allows it to maintain the H_2 production.

Acknowledgments

This work was financially supported by SENER-CONACYT (251801) and PAPIIT-UNAM (IN-101916) projects. J. A. Mendoza-Nieto thanks DGAPA-UNAM for financial support. Authors thank to A. Tejeda for technical help.

References

[1] S.J. Chapman, M. Thurlow, The influence of climate on CO_2 and CH_4 emissions from organic soils, Agric. For. Meteorol. 79 (1996) 205–217, http://dx.doi.org/10.1016/0168-1923(95)02283-X.
[2] K.B. Bartlett, R.C. Harriss, Review and assessment of methane emissions from wetlands, Chemosphere 26 (1993) 261–320, http://dx.doi.org/10.1016/0045-6535(93)90427-7.
[3] S. Ma'mun, H.F. Svendsen, K.A. Hoff, O. Juliussen, Selection of new absorbents for carbon dioxide capture, Energy Convers. Manage. 48 (2007) 251–258, http://dx.doi.org/10.1016/j.enconman.2006.04.007.
[4] D.T. Allen, V.M. Torres, J. Thomas, D.W. Sullivan, M. Harrison, A. Hendler, S.C. Herndon, C.E. Kolb, M.P. Fraser, A.D. Hill, B.K. Lamb, J. Miskimins, R.F. Sawyer, J.H. Seinfeld, Measurements of methane emissions at natural gas production sites in the United States, Proc. Natl. Acad. Sci. 110 (2013) 17768–17773, http://dx.doi.org/10.1073/pnas.1304880110.
[5] S. Nanda, S.N. Reddy, S.K. Mitra, J.A. Kozinski, The progressive routes for carbon capture and sequestration, Energy Sci. Eng. 4 (2016) 99–122, http://dx.doi.org/10.1002/ese3.117.
[6] M.C.J. Bradford, M.A. Vannice, CO_2 reforming of CH_4, Catal. Rev. 41 (1999) 1–42, http://dx.doi.org/10.1081/CR-100101948.
[7] J.D. Holladay, J. Hu, D.L. King, Y. Wang, An overview of hydrogen production technologies, Catal. Today 139 (2009) 244–260, http://dx.doi.org/10.1016/j.cattod.2008.08.039.
[8] M. Momirlan, T. Veziroğlu, Recent directions of world hydrogen production, Renew. Sustain. Energy Rev. 3 (1999) 219–231, http://dx.doi.org/10.1016/S1364-0321(98)00017-3.
[9] Y. Cui, H. Zhang, H. Xu, W. Li, Kinetic study of the catalytic reforming of CH_4 with CO_2 to syngas over Ni/α-Al_2O_3 catalyst: the effect of temperature on the reforming mechanism, Appl. Catal. A Gen. 318 (2007) 79–88, http://dx.doi.org/10.1016/j.apcata.2006.10.044.
[10] C.A.M. Abreu, D.A. Santos, J.A. Pacífico, N.M. Lima Filho, Kinetic evaluation of methane-carbon dioxide reforming process based on the reaction steps, Ind. Eng. Chem. Res. 47 (2008) 4617–4622, http://dx.doi.org/10.1021/ie071546y.
[11] A. Wolfbeisser, O. Sophiphun, J. Bernardi, J. Wittayakun, K. Föttinger, G. Rupprechter, Methane dry reforming over ceria-zirconia supported Ni catalysts, Catal. Today 277 (2016) 234–245, http://dx.doi.org/10.1016/j.cattod.2016.04.025.
[12] B. Djebarri, V.M. Gonzalez-Delacruz, D. Halliche, K. Bachari, A. Saadi, A. Caballero, J.P. Holgado, O. Cherifi, Promoting effect of Ce and Mg cations in Ni/Al catalysts prepared from hydrotalcites for the dry reforming of methane, React. Kinet. Mech. Catal. 111 (2014) 259–275, http://dx.doi.org/10.1007/s11144-013-0646-2.
[13] A.F. Lucrédio, E.M. Assaf, Cobalt catalysts prepared from hydrotalcite precursors and tested in methane steam reforming, J. Power Sources 159 (2006) 667–672, http://dx.doi.org/10.1016/j.jpowsour.2005.10.108.
[14] A. Sauvet, J.T.S. Irvine, Catalytic activity for steam methane reforming and physical characterisation of $La_{1-x}Sr_xCr_{1-y}Ni_yO_{3-\delta}$, Solid State Ionics 167 (2004) 1–8, http://dx.doi.org/10.1016/j.ssi.2003.11.021.
[15] M.H. Halabi, J.M. De Croon, J. Van Der Schaaf, P.D. Cobden, J.C. Schouten, Reactor modeling of sorption-enhanced autothermal reforming of methane. Part I: performance study of hydrotalcite and lithium zirconate-based processes, Chem. Eng. J. 168 (2011) 872–882, http://dx.doi.org/10.1016/j.cej.2011.02.015.
[16] M.H. Halabi, M.H.J.M. de Croon, J. van der Schaaf, P.D. Cobden, J.C. Schouten, Reactor modeling of sorption-enhanced autothermal reforming of methane. Part II: effect of operational parameters, Chem. Eng. J. 168 (2011) 883–888, http://dx.doi.org/10.1016/j.cej.2011.02.016.
[17] J.R. Hufton, S. Mayorga, S. Sircar, Sorption-enhanced reaction process for hydrogen production, AIChE J. 45 (1999) 248–256, http://dx.doi.org/10.1002/aic.690450205.
[18] Y. Li, Q. Fu, M. Flytzani-Stephanopoulos, Low-temperature water-gas shift reaction over Cu- and Ni-loaded cerium oxide catalysts, Appl. Catal. B Environ. 27 (2000) 179–191, http://dx.doi.org/10.1016/S0926-3373(00)00147-8.
[19] Q. Fu, W. Deng, H. Saltsburg, M. Flytzani-Stephanopoulos, Activity and stability of low-content gold–cerium oxide catalysts for the water–gas shift reaction, Appl. Catal. B Environ. 56 (2005) 57–68, http://dx.doi.org/10.1016/j.apcatb.2004.07.015.
[20] A. Sandoval, A. Gómez-Cortés, R. Zanella, G. Díaz, J.M. Saniger, Gold nanoparticles: support effects for the WGS reaction, J. Mol. Catal. A Chem. 278 (2007) 200–208, http://dx.doi.org/10.1016/j.molcata.2007.09.014.
[21] A. López Ortiz, M.A. Escobedo Bretado, J. Salinas Gutiérrez, M. Meléndez Zaragoza, R.H. Lara Castro, V. Collins Martínez, Na_2ZrO_3 stability under reforming/regeneration cycles during the steam reforming of ethanol with CO_2 absorption, Int. J. Hydrogen Energy 40 (2015) 17192–17199, http://dx.doi.org/10.1016/j.ijhydene.2015.08.020.
[22] D.Y. Aceves Olivas, M.R. Baray Guerrero, M.A. Escobedo Bretado, M. Marques da Silva Paula, J. Salinas Gutiérrez, V. Guzmán Velderrain, A. López Ortiz, V. Collins-Martínez, Enhanced ethanol steam reforming by CO_2 absorption using CaO, CaO*MgO or Na_2ZrO_3, Int. J. Hydrogen Energy 39 (2014) 16595–16607, http://dx.doi.org/10.1016/j.ijhydene.2014.04.156.
[23] K. Essaki, T. Muramatsu, M. Kato, Effect of equilibrium-shift in the case of using lithium silicate pellets in ethanol steam reforming, Int. J. Hydrogen Energy 33 (2008) 6612–6618, http://dx.doi.org/10.1016/j.ijhydene.2008.08.025.
[24] S.D. Kenarsari, D. Yang, G. Jiang, S. Zhang, J. Wang, A.G. Russell, Q. Wei, M. Fan, Review of recent advances in carbon dioxide separation and capture, RSC Adv. 3 (2013) 22739–22773, http://dx.doi.org/10.1039/c3ra43965h.
[25] J. Montoya, E. Romero-Pascual, C. Gimonc, P. Del Ángel, A. Monzón, Methane reforming with CO_2 over Ni/ZrO_2–CeO_2 catalysts prepared by sol–gel, Catal. Today 63 (2000) 71–85, http://dx.doi.org/10.1016/S0920-5861(00)00447-8.
[26] J.-M. Lavoie, Review on dry reforming of methane, a potentially more environmentally-friendly approach to the increasing natural gas exploitation, Front. Chem. 2 (2014), http://dx.doi.org/10.3389/fchem.2014.00081.
[27] T.F. Wall, Combustion processes for carbon capture, Proc. Combust. Inst. 31 (2007) 31–47, http://dx.doi.org/10.1016/j.proci.2006.08.123.
[28] J. Gibbins, H. Chalmers, Carbon capture and storage, Energy Policy 36 (2008) 4317–4322, http://dx.doi.org/10.1016/j.enpol.2008.09.058.
[29] M. Kato, K. Essaki, K. Nakagawa, Y. Suyama, K. Terasaka, CO_2 absorption properties of lithium ferrite for application as a high-temperature CO_2 absorbent, J. Ceram. Soc. Japan 113 (2005) 684–686, http://dx.doi.org/10.2109/jcersj.113.684.
[30] A. Samanta, A. Zhao, G.K.H. Shimizu, P. Sarkar, R. Gupta, Post-combustion CO_2 capture using solid sorbents: a review, Ind. Eng. Chem. Res. 51 (2012) 1438–1463, http://dx.doi.org/10.1021/ie200686q.
[31] M.J. Moreno-Ramírez, I.C. Romero-Ibarra, J. Ortiz- Landeros, H. Pfeiffer, Alkaline and alkaline-earth ceramic oxides for CO_2 capture, separation and subsequent catalytic chemical conversion, CO_2 Sequestration Valorization, InTech, 2014, http://dx.doi.org/10.5772/57444.
[32] T. Nakagawa, K. Ohashi, A novel method of CO_2 capture from high temperature gases, J. Electrochem. Soc. 145 (1998) 1344–1346, http://dx.doi.org/10.1149/1.1838462.
[33] J. Wang, L. Huang, R. Yang, Z. Zhang, J. Wu, Y. Gao, Q. Wang, D. O'Hare, Z. Zhong, Recent advances in solid sorbents for CO_2 capture and new development trends, Energy Environ. Sci. 7 (2014) 3478–3518, http://dx.doi.org/10.1039/C4EE01647E.
[34] O. Ovalle-Encinia, J.A. Mendoza-Nieto, J. Ortiz-Landeros, H. Pfeiffer, $Ce_{0.8}Sm_{0.15}Sr_{0.05}O_2$ as possible oxidation catalyst and assessment of the CaO addition in the coupled CO Oxidation–CO_2 capture process, Ind. Eng. Chem. Res. 56 (2017) 6124–6130, http://dx.doi.org/10.1021/acs.iecr.6b04872.
[35] J.A. Mendoza-Nieto, H. Pfeiffer, Thermogravimetric study of sequential carbonation and decarbonation processes over Na_2ZrO_3 at low temperatures (30–80 °C): relative humidity effect, RSC Adv. 6 (2016) 66579–66588, http://dx.doi.org/10.1039/C6RA12533F.
[36] J.A. Mendoza-Nieto, E. Vera, H. Pfeiffer, Methane reforming process by means of a carbonated-Na_2ZrO_3 catalyst, Chem. Lett. 45 (2016) 3–6, http://dx.doi.org/10.1246/cl.160136.
[37] A. Cruz-Hernández, J.A. Mendoza-Nieto, H. Pfeiffer, NiO-CaO materials as promising catalysts for hydrogen production through carbon dioxide capture and subsequent dry methane reforming, J. Energy Chem. (2017), http://dx.doi.org/10.1016/j.jechem.2017.07.002.
[38] V.L. Mejía-Trejo, E. Fregoso-Israel, H. Pfeiffer, Textural, structural, and CO_2 chemisorption effects produced on the lithium orthosilicate by its doping with sodium ($Li_{4-x}Na_xSiO_4$), Chem. Mater. 20 (2008) 7171–7176, http://dx.doi.org/10.1021/cm802132t.
[39] S. Lowell, J.E. Shields, M.A. Thomas, M. Thommes, Characterization of Porous Solids and Powders: Surface Area, Pore Size and Density, Springer, Netherlands, Dordrecht, 2004, http://dx.doi.org/10.1007/978-1-4020-2303-3.
[40] G.G. Santillán-Reyes, H. Pfeiffer, Analysis of the CO_2 capture in sodium zirconate (Na_2ZrO_3). Effect of the water vapor addition, Int. J. Greenh. Gas Control 5 (2011) 1624–1629, http://dx.doi.org/10.1016/j.ijggc.2011.09.009.
[41] H. Pfeiffer, C. Vázquez, V.H. Lara, P. Bosch, Thermal behavior and CO_2 absorption of $Li_{2-x}Na_xZrO_3$ solid solutions, Chem. Mater. 19 (2007) 922–926, http://dx.doi.org/10.1021/cm0623965.
[42] I. Alcérreca-Corte, E. Fregoso-Israel, H. Pfeiffer, CO2 absorption on Na_2ZrO_3: a

kinetic analysis of the chemisorption and diffusion processes, J. Phys. Chem. C 112 (2008) 6520–6525, http://dx.doi.org/10.1021/jp710475g.
[43] J. Ortiz-Landeros, T.L. Ávalos-Rendón, C. Gómez-Yáñez, H. Pfeiffer, Analysis and perspectives concerning CO_2 chemisorption on lithium ceramics using thermal analysis, J. Therm. Anal. Calorim. 108 (2012) 647–655, http://dx.doi.org/10.1007/s10973-011-2063-y.
[44] J.-W. Kim, H.-G. Lee, Thermal and carbothermic decomposition of Na_2CO_3 and Li_2CO_3, Metall. Mater. Trans. B 32 (2001) 17–24, http://dx.doi.org/10.1007/s11663-001-0003-0.
[45] L. Martínez-dlCruz, H. Pfeiffer, Cyclic CO_2 chemisorption–desorption behavior of Na_2ZrO_3: structural, microstructural and kinetic variations produced as a function of temperature, J. Solid State Chem. 204 (2013) 298–304, http://dx.doi.org/10.1016/j.jssc.2013.06.014.